Numerical Investigation on Shear Driven Cavity Flow by the Constrained Interpolated Profile Lattice Boltzmann Method

*C. S. NOR AZWADI, M. H. Al-MOLA and S. AGUS
Department of Thermo-fluid
Universiti Teknologi Malaysia
81310 UTM Skudai, Johor
MALAYSIA
azwadi@fkm.utm.my http://www.fkm.utm.my/~azwadi

Abstract: - In this paper, we proposed a combination of lattice Boltzmann and finite difference schemes to simulate an incompressible fluid flow problem. Our model applies the constrained interpolated profile method to solve the advection term in the governing lattice Boltzmann equation. Compared with the conventional lattice Boltzmann scheme, the current scheme is more accurate. In addition, the proposed model requires less mesh size for the computational at various conditions compared to other lattice Boltzmann models. Simulation of lid-driven cavity flow whose Reynolds number up to 1000 were carried out in order to validate the proposed approach. Numerical results show excellent agreement with those obtained by the conventional computational fluid dynamics approaches. We then extend our computation on the behavior of vortex inside a shallow lid-driven cavity flow at various aspect ratios. We found that the formation, strength and size of primary and secondary vortices are significantly affected by the value of aspect ratio and Reynolds numbers. Good comparisons were obtained when the results are compared with those published in the literature. This indicates that the proposed approach is a reliable alternative computational scheme in predicting various types of fluid flow problem.

Key-Words: - lattice Boltzmann, distribution function, BGK collision, constrained interpolated profile, lid-driven cavity flow

1 Introduction

Lattice Boltzmann method (LBM) is a relatively new and promising numerical method for predicting complex fluid systems and has attracted interest from researchers in computational physics. Each month several papers appear with new models, investigate of known models or methodically interesting applications [1-3]. Unlike other traditional computational fluid dynamics (CFD) methods, which solve the conservation equations of macroscopic properties (i.e., mass, momentum, and energy) numerically, LBM models the fluid consisting of fictive particles. These particles perform consecutive propagation and collision processes over a discrete lattice mesh or grid.

Historically, LBM was derived from the lattice gas automata (LGA) [4]. Consequently, LBM inherits some features from it precursor, the LGA method. The first LBM model was a floating-point version of its LGA counterpart. Each particle in LGA model (represented by single bit Boolean integer) was replaced by a single particle distribution function represented by a floating-point number. The lattice structure and the evolution rule remain the same. One important improvement to enhance the computational efficiency has been made for the LBM was that the linearization of collision operator. The uniform lattice structure was remaining unchanged.

The LBM has a number of advantages over other conventional computational fluid dynamics approaches. The algorithm is simple and can be implemented with a kernel of just a few hundred lines. The algorithm can also be easily modified to allow for the application of other, more complex simulation components. For example, the LBM can be extended to describe the evolution of binary mixtures, or extended to allow for more complex boundary conditions. Thus the LBM is an ideal tool in fluid simulation.

Although promising, the current LBM still have few shortcomings that limit its general application as a practical computational fluid dynamics tool. One of these shortcomings, which is specifically addressed in this paper, is it's constrained to second order accuracy in space and time. Due to this restraint, the standard LBM has great difficulty in simulating fluid flow problem under critical conditions that require higher order accuracy either in space or time. Since He and Luo [5] and Abe [6] demonstrated that the lattice Boltzmann equation is a discretized form of the continuous Boltzmann equation, and the discretization of physical space is not coupled with the discretization of momentum space, any standard numerical techniques can serve

the purpose of solving the discrete Boltzmann equation. It is not surprising that the well-known finite different has being introduced in order to improve the accuracy of the conventional LBM.

The first finite different LBM (FDLBM) was due to Reider and Sterling [7], and was examined by Cao et al. [8] in more detail. FDLBM was further extended to curvilinear coordinates with non-uniform grids by Mei and Shyy [9]. The study of FDLBM is still in progress [10-12].

In this research, works have been done on the improvement of the FDLBM. The advection term in the governing equation of is solved using the constrained interpolated profile method [13] which is expected to contribute third order accuracy in space. In order to demonstrate the efficiency the current approach, we carried out numerical investigation of shear driven cavity flow up to Reynolds number of 1000 and compared the results with other type of FDLBM and 'benchmark' solutions by Ghia et al [14]. After we got confidence with the formulation, we extend our investigation to shear driven flow in a shallow cavity.

This paper is organized as follow. In the next section, the formulation of LBM is described in detail. In the sequence section, the contrained interpolated profile is employed in the governing equation of LBM to simulation shear driven flow in a cavity. The final section concludes this study.

2 Isothermal Lattice Boltzmann Model

In two-dimensional space, the governing equation of the model is written as

$$\frac{\partial f}{\partial t}+\mathbf{c}\frac{\partial f}{\partial \mathbf{x}}=\Omega(f) \tag{1}$$

where $f=f(\mathbf{c},\mathbf{x},t)$ is the density distribution function with its probable microscopic velocity $\mathbf{c}$ and used to calculate macroscopic values of density and velocity field. $\Omega(f)$ on the right hand side represents the collision function of the particle distribution functions.

Any solution to Eq. (1) requires an expression for the collision operator $\Omega(f)$. If the collision is to conserve mass, momentum and energy, it is required that

$$\int \begin{vmatrix} 1 \\ \mathbf{c} \\ \mathbf{c}^2 \end{vmatrix} \Omega d\mathbf{c}=0 \tag{2}$$

However, the expression for $\Omega(f)$ is too complex to be solved [15]. Any replacement of collision must satisfy the conservation laws as expressed in Eq. (2). The idea behind this replacement is that large amount of detail of two-body interaction is not likely to influence significantly the values of many experimental measured quantities [16].

There are a few version of collision operator published in the literature. However, the most well accepted version due to its simplicity and efficiency is the Bhatnagar Gross Crook (BGK) collision model [17] with a single relaxation time. The equation that represents this model is given by

$$\Omega(f)=-\frac{f-f^{eq}}{\tau} \tag{3}$$

where f^{eq} is the equilibrium distribution function and τ is the time to reach equilibrium condition during collision process and is often called the relaxation time. Another function of τ is to control the amount of distribution function relaxes to equilibrium state on every collision stage.

Nor Azwadi et al. [18] have recently shown that the discretized equilibrium distribution function can be obtained by applying the Gauss-Hermite quadrature procedure for the calculation of f^{eq} velocity moments. As a result, a 2-dimensional 9-velocity, D2Q9 lattice model, as shown in Fig. 1, is obtained.

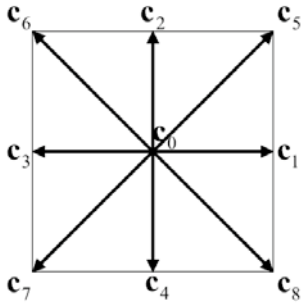

Fig. 1 Lattice structure for D2Q9 model.

The corresponding expression for the equilibrium density distribution function is given by

$$f_i^{eq}=\rho\omega_i\left[1+3(\mathbf{c}\cdot\mathbf{u})+4.5(\mathbf{c}\cdot\mathbf{u})^2-1.5\mathbf{u}^2\right] \tag{4}$$

where $\omega_0=4/9$, $\omega_{1-4}=1/9$ and $\omega_{5-8}=1/36$. After discretisation in velocity space, the Boltzmann equation with the BGK collision function can be rewritten as follow

$$\frac{\partial f_i}{\partial t} + \mathbf{c}_i \frac{\partial f_i}{\partial \mathbf{x}} = -\frac{f_i - f_i^{eq}}{\tau} \tag{5}$$

and well known as BGK lattice Boltzmann equation.

The macroscopic variables such as density ρ and velocity $\mathbf{u}$ can be evaluated as the moment to the distribution function

$$\rho = \int_{i=0}^{8} f_i d\mathbf{c} \quad \text{and} \quad \rho\mathbf{u} = \int_{i=0}^{8} \mathbf{c}_i f_i d\mathbf{c} \tag{6}$$

Through a multiscaling expansion, the mass and momentum equation can be derived from the D2Q9. The detail derivation can be referred to Nor Azwadi et al [19] and will not be shown here

$$\nabla \cdot \mathbf{u} = 0 \tag{7}$$

$$\frac{\partial \mathbf{u}}{\partial t} + \mathbf{u}\nabla \cdot \mathbf{u} = -\frac{1}{\rho}\nabla p + \upsilon \nabla^2 \mathbf{u} \tag{8}$$

The viscosity in this model can be related to the time relaxation as below

$$\upsilon = \frac{1}{3}\tau \tag{9}$$

3 Constrained Interpolated Profile (CIP) Method

The CIP method was proposed by Yabe et al [20] and has been highly proven to be a universal solver for hyperbolic type equations. In this section, we briefly discuss the key points of CIP scheme in one-dimension case.

We consider a linear hyperbolic equation to be solved in the following term

$$\frac{\partial f}{\partial t} + c\frac{\partial f}{\partial x} = 0 \tag{10}$$

The theoretical solution of Eq. (10) is obtained by shifting a profile

$$f(x, t+\Delta t) = f(x - c\Delta t, t) \tag{11}$$

this represents a simple translation of profiles with velocity c. If we differentiate Eq. (10) with spatial variable x, then we get

$$\frac{\partial f_x}{\partial t} + c\frac{\partial f_x}{\partial x} = 0 \tag{12}$$

where $f_x = \partial f / \partial x$. Equation (12) coincides with Eq. (10) and represents the translation of f with velocity c. The novel idea behind the CIP approach is, we trace the time evolution of both f and f_x using Eqs. (10) and (12) and the profile at each node after one step are specified according to Eq. (11). With this restriction, we can greatly reduce the numerical diffusion when we construct the profile [21].

In the CIP method, spatial quantities in the grid interval are approximated with constrained polynomial using f and f_x at neighboring grid points as follow

$$F_i(x) = a_i X^3 + b_i X^2 + f_{x,i} X + f_i \tag{13}$$

where $X = x - x_i$. The coefficients of a_i and b_i in Eq. (13) are determined so that the interpolation function and its first derivatives are continuous at both ends. As a result, we have

$$a_i = \frac{f_{x,i} + f_{x,i-1}}{\Delta x^2} - \frac{2(f_i + f_{i-1})}{\Delta x^3} \tag{14}$$

$$b_i = \frac{2(f_{x,i} + f_{x,i-1})}{\Delta x} - \frac{3(f_i + f_{i-1})}{\Delta x^2} \tag{15}$$

where $\Delta x = x_i - x_{i-i}$. Once $F_i(x)$ are determined for all grid intervals, the spatial derivative is calculated as

$$F_{x,i}(x) = 3a_i X^2 + 2b_i X + f_{x,i} \tag{16}$$

After all, the advected profile is given by

$$f_i^{n+1} = F_i(x - \xi) = a_i(\xi)^3 + b_i(\xi)^2 + f_{x,i}(\xi) + f_i \tag{17}$$

$$f_{x,i}^{n+1} = F_{x,i}(x - \xi) = 3a_i(\xi)^2 + 2b_i(\xi) + f_{x,i} \tag{18}$$

where $\xi = c\Delta t$ and the superscript n indicates the time.

We first apply CIP method to the propagation of a square wave. Figure 2a-c shows the plots of profile obtained from CIP, Lax-Wendroff and first order upwind methods. As expected, CIP scheme shows smaller diffusion and dispersion errors compared to the other solution methods. We then calculated the average percentage of error produced by each method and summarized in Table 1.

From Figure 2 and Table 1, we can see that the CIP method gives the best accuracy compared to

other well-known numerical solution to advection equation.

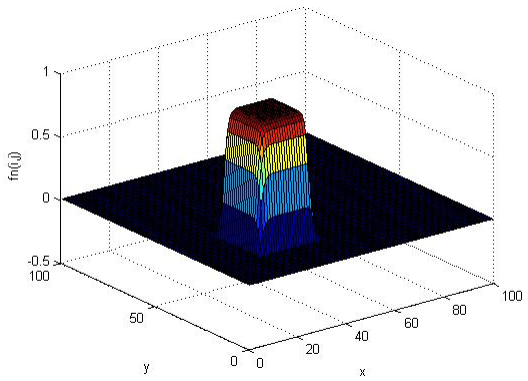

(a) CIP solution

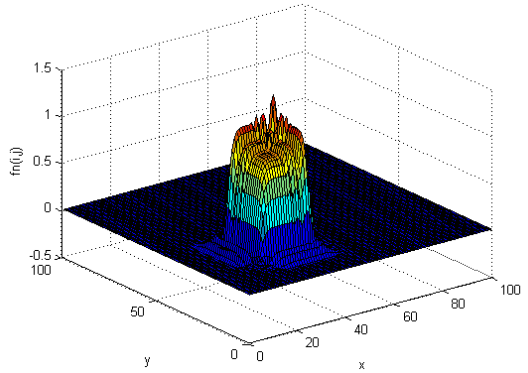

(b) Lax-Wendroff solution

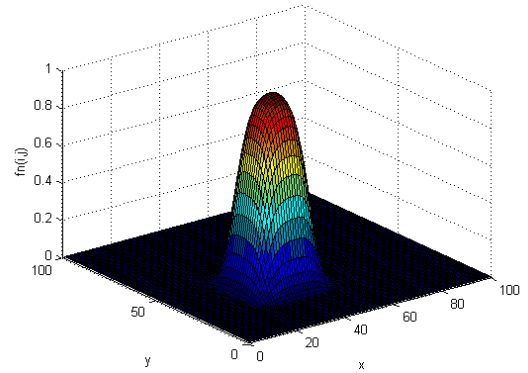

(c) First order upwind scheme solution

Fig. 2 Numerical solution to advection equation

Tab. 1 Computed average error for every solution method

Solution Method	First order upwind	Lax-Wendroff	CIP
Average Error (%)	6.820	5.421	1.454

4 Two-Dimension CIP Lattice Boltzmann Method

In the formulation of CIPLBM scheme, the governing equation is readily split into advection and non-advection phase (Refer Eq. (1)). The right hand side of the equation, the non-advection phase or collision term specifically, can be directly solved without any difficulty. On the other hand, the equation in the advection phase will be solved using the CIP method discussed in the previous section.

The evolution of advection and collision phase can be rewritten separately as follow

$$\frac{\partial f_i}{\partial t} = -\mathbf{c}_i \frac{\partial f_i}{\partial \mathbf{x}} \tag{19}$$

and

$$\frac{\partial f_i}{\partial t} = -\frac{f_i - f_i^{eq}}{\tau} \tag{20}$$

We then differentiate Eqs. (19) and (20) with spatial variables x and y gives

$$\frac{\partial f_{x,i}}{\partial t} = -\mathbf{c}_i \frac{\partial f_{x,i}}{\partial \mathbf{x}} \tag{21}$$

$$\frac{\partial f_{y,i}}{\partial t} = -\mathbf{c}_i \frac{\partial f_{y,i}}{\partial \mathbf{x}} \tag{22}$$

and

$$\frac{\partial f_{x,i}}{\partial t} = -\frac{f_{x,i} - f_{x,i}^{eq}}{\tau} \tag{23}$$

$$\frac{\partial f_{y,i}}{\partial t} = -\frac{f_{y,i} - f_{y,i}^{eq}}{\tau} \tag{24}$$

where $f_x = \partial f / \partial x$ and $f_y = \partial f / \partial y$.

In the computation at two-dimensional space, distribution function in the element grid interval are approximated as follow

$$F_i(x,y) = \left[(a1X + a2Y + a3)X + a4Y + f_{xi}\right]X + \left[(a5Y + a6X + a7)Y + f_{xi}\right]Y + f_i \tag{25}$$

where

$$a1 = \frac{-2d_m + \left(f_{xi,m-1,n} + f_{xi,m,n} \right)}{\Delta x^3} \tag{26}$$

$$a2 = \frac{a8 - d_{xn}\Delta x}{\Delta x^2 \Delta y} \tag{27}$$

$$a3 = \frac{-3d_n - \left(f_{xi,m-1,n} + 2f_{xi,m,n} \right)\Delta x}{\Delta x^2} \tag{28}$$

$$a4 = \frac{-a8 + d_{xn}\Delta x + d_{yn}\Delta y \Delta x}{\Delta x \Delta x} \tag{29}$$

$$a5 = \frac{-2d_n + \left(f_{yi,m,n+1} \right)\Delta y}{\Delta y^3} \tag{30}$$

$$a6 = \frac{a8 - d_{ym}\Delta y}{\Delta x \Delta y^2} \tag{31}$$

$$a7 = \frac{3d_m + \left(f_{yi,m,n-1} + 2f_{yi,m,n} \right)\Delta y}{\Delta y^2} \tag{32}$$

$$a8 = f_{i,m,n} - f_{i,m-1,n} - f_{i,m,n-1} + f_{i,m-1,n-1} \tag{33}$$

here $d_m = f_{i,m,n} - f_{i,m-1,n}$, $d_n = f_{i,m,n} - f_{i,m,n-1}$ and m and n refer to horizontal and vertical direction in phase space.

The spatial derivatives are calculated as

$$F_{xi}(x,y) = \left(3a1X + 2a2Y + a3\right)X + \left(a4 + a6Y\right)Y + f_{xi} \tag{34}$$

$$F_{yi}(x,y) = \left(a2X + a4\right)X + \left(3a5Y + 2a6X + 2a7\right)Y + f_{yi} \tag{35}$$

In two-dimensional case, the advected profile is approximated as follow

$$f_i^n = F_i\left(x + \xi_{xi}, y + \xi_{yi}\right) \tag{36}$$

$$f_{xi}^n = F_{xi}\left(x + \xi_{xi}, y + \xi_{yi}\right) \tag{37}$$

$$f_{yi}^n = F_{yi}\left(x + \xi_{xi}, y + \xi_{yi}\right) \tag{38}$$

where $\xi_{xi} = -c_{xi}\Delta t$ and $\xi_{yi} = -c_{yi}\Delta t$.

In summary, the evolution of CIP-LBM consists of three steps. The initial value of f_i, f_{xi} and f_{yi} are specified at each grid point (m,n). Then the system evolves in the following steps;

Since the pre-advected value of f_i, f_{xi} and f_{yi} are known on each grid, the constrained interpolation process can be completed according to Eqs. (25), (34) and (35).

After the interpolation, advection takes place, and f_i^n, f_{xi}^n and f_{yi}^n are obtained.

The values of f_i^{n+1}, f_{xi}^{n+1} and f_{yi}^{n+1} on the mesh grid are computed from the newly advected values in step 2. Then the interpolation and the advection processes are repeated.

5 Simulation Results

In this section, we apply the CIPLBM discussed in the proceeding section to predict the flow structure inside a lid-driven square cavity. The obtained results are then compared with those predicted from first order upwind scheme lattice Boltzmann method. The purpose of the comparison is to demonstrate the capability of CIPLBM to produce an excellent result compared with the first order upwind lattice Boltzmann method under the same number of grids needed to interpolate profile between the two neighboring grids.

The lid-driven cavity flow has been used as a benchmark problem for many numerical methods due to its simple geometry and complicated flow behaviours. It is usually very difficult to capture the flow phenomena near the singular points at the corners of the cavity. In the simulation, the Reynolds number is chosen to be 100, 400 and 1000. The 50 × 50 uniform mesh is used for both methods.

Figures 3(a)-3(c) show the plots of vertical and horizontal velocity profile at the mid-height and mid-width of the cavity respectively. As can be seen from the figure, the results computed from the CIPLBM are very close agreement with the benchmark solution of Ghia et al. [14]. However, at the highest Reynolds number computations, some deviations can be seen due to low spatial resolution, but still the CIPLBM is able to show the correct profile.

Figures 4(a)-4(c) show plots of stream function for the Reynolds numbers considered obtained from CIP prediction. It is apparent that the flow structure is in good agreement with the previous work of Ghia et al.

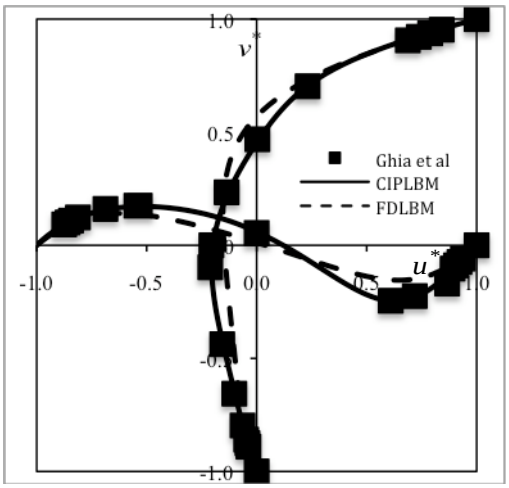

(a)

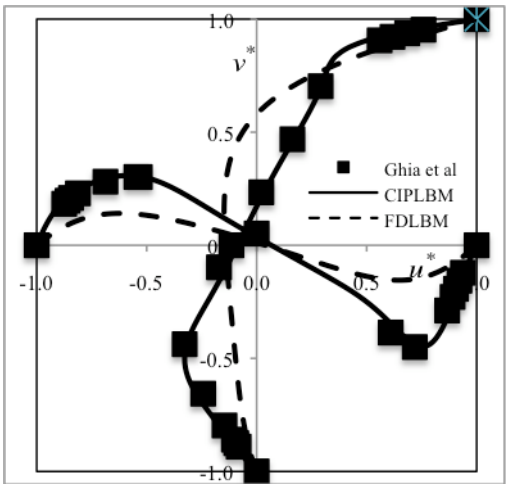

(b)

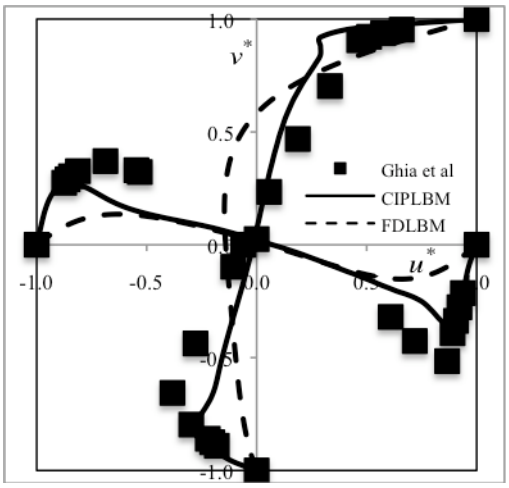

(c)

Fig. 3 Velocity component plots for (a) $Re = 100$, (b) $Re = 400$ and (c) $Re = 1000$

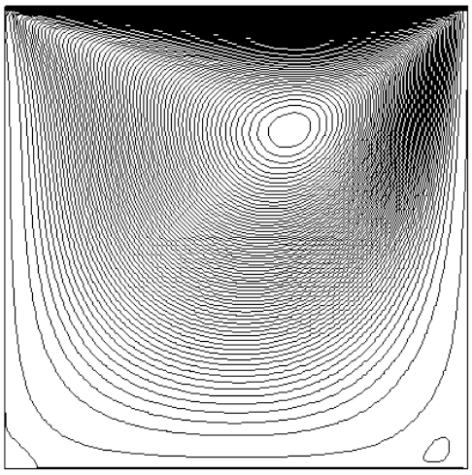

(a)

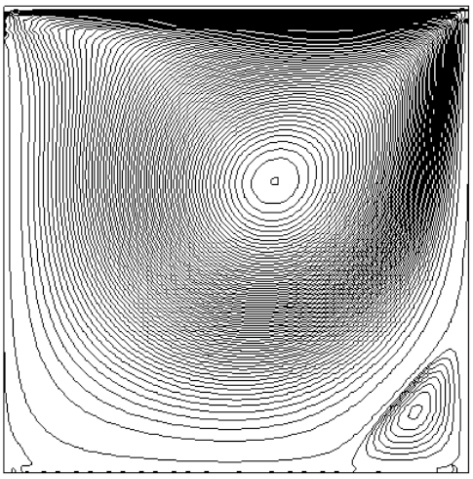

(b)

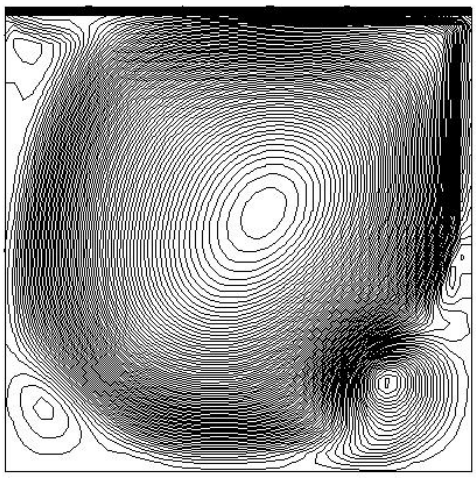

(c)

Fig. 4 Streamline plots for (a) $Re = 100$, (b) $Re = 400$ and (c) $Re = 1000$

For low Reynolds number simulation, $Re = 100$, the center of vortex is located at about one-third of the cavity depth from the top. As Re increases, the primary vortex moves towards the center of cavity and increasing circular. In addition to the primary, a pair of counterrotating eddies develop at the lower corners of the cavity.

From the results presented above, we can see that the CIPLBM produced an excellent agreement with those published in the literature.

After we gain confidence in our computational method, we carry out investigation of flow structure in a shear driven shallow cavity. The aspect ratio defined in current study is $D = w/h$ where w and h represent the width and height of the cavity respectively. Three values of aspect ratio ($D = 1.5$, 2 and 3) are considered and the flow behavior at Reynolds numbers of 100, 400 and 1000 are investigated for every value of *D*. We present our results based on the plots of streamlines to discuss the vortex behavior in the system under the effect of aspect ratio and Reynolds number.

The simulation set up for every condition is tabulated in Table 2.

Tab. 2 Initial setup for the computation of shallow lid-driven cavity flow using CIPLBM

Reynolds No.	Aspect Ratio	Mesh size
100	1.5	75 x 50
400		
1000		
100	2.0	100 x 50
400		
1000		
100	3.0	150 x 50
400		
1000		

The simulations were considered to have reached a steady state condition when the r.m.s change in horizontal and vertical velocity decreased to a magnitude of 10^6 or less.

Figs. 5(a)-(c) show the streamlines of cavity with aspect ratio 1.5. These three figures corresponds to *Re* = 100, 400 and 1000 with mesh sizes mentioned in Tab. 2. As can be seen from the figures, for low Reynolds number simulation, a counter-rotating vortex is formed at the one-third from the top moving lid. As the Reynolds number increases, the center of the primary eddy begin to move downwards and achieved steady state at the center of the system for *Re* = 1000. The secondary eddies are believed started to develop at *Re* = 100. However, we failed to capture this phenomenon due to low spatial resolution. As we increase the Reynolds numbers, the secondary vortices can be clearly seen at the bottom corners of the cavity. The left secondary vortex shows bigger in size due to higher force drags the vortex upwards compared to the right region. As a result, the center of the secondary vortex on the left side is shifted upwards and formed at the one-third from the top lid of the cavity.

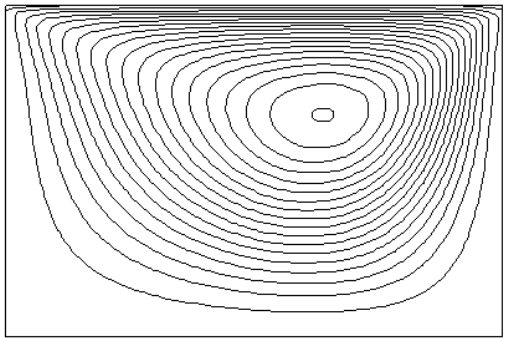

(a)

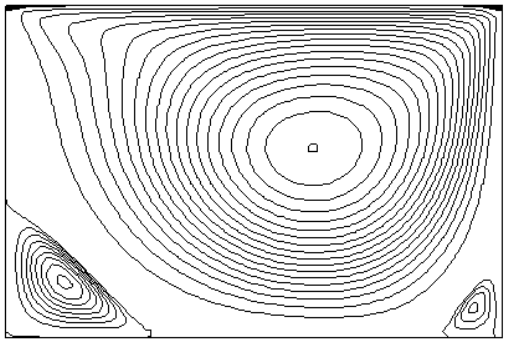

(b)

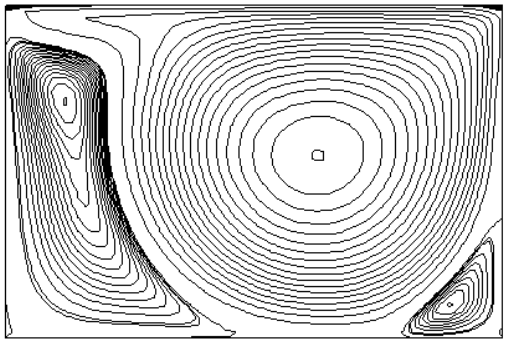

(c)

Fig. 5 Streamline plots for (a) $Re = 100$, (b) $Re = 400$ and (c) $Re = 1000$ at aspect ratio of 1.5.

For the case where the aspect ratio is 2.0, a grid size of 50 x 100 was employed. Figs. 6(a)-6(b) show that the primary vortex center descends to the center of the cavity with increased strength as the Reynolds number increases. From the figure, two secondary vortices of different sizes are visible at the lower

corners of the cavity with the left vortex being bigger than the right vortex due to the flow direction from the right corner to the left corner. The difference in size becomes obvious with increasing Reynolds numbers. This phenomenon affects the position of the center of primary vortex which is shifted to the right of the cavity system.

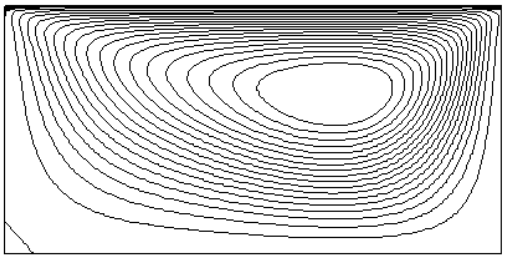

(a)

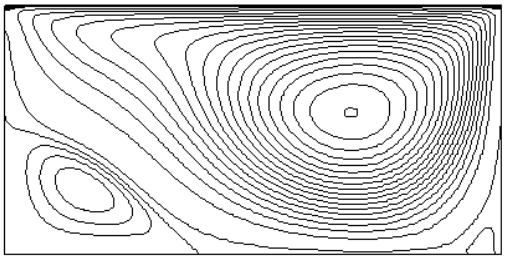

(b)

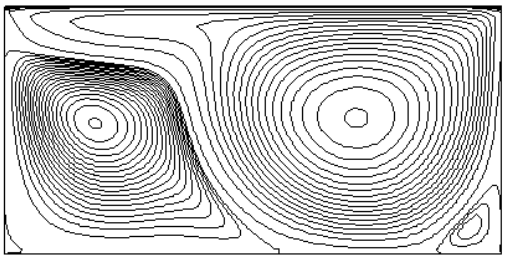

(c)

Fig. 6 Streamline plots for (a) $Re = 100$, (b) $Re = 400$ and (c) $Re = 1000$ at aspect ratio of 2.0.

For an aspect ratio of 3.0 which represent a more shallow cavity, the simulation employed 50 x 150 grid system. As Reynolds numbers increases, Figs. 7(a)-7(c) show that the primary vortex began to split into two vortices. However, very small secondary vortices are observed at the bottom corners even when the Reynolds numbers increases. Hence, it can be said that the enlarged cavity in the flow direction will supress the generation of vortices at the corners. The secondary vortices can only be clearly seen at *Re* = 1000 simulation. However, it's shape is elongated horizontally due to the formation of primary vortex on top of it due to dominant inertia force in this range of Reynolds number. All of these observations are in good agreement with the previously published results on the literature [22-25].

From the results presented above, we can say that the CIPLBM is a reliable alternative numerical method which is capable to capture the critical points in the tested problem.

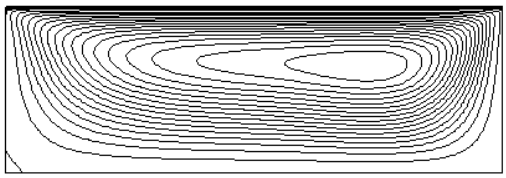

(a)

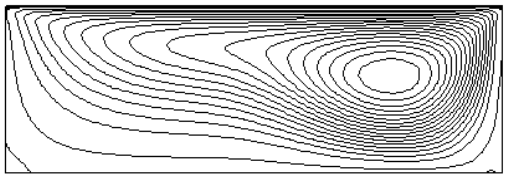

(b)

(c)

Fig. 7 Streamline plots for (a) $Re = 100$, (b) $Re = 400$ and (c) $Re = 1000$ at aspect ratio of 3.0.

5 Conclusion

In this paper, the phenomenon of an incompressible fluid flow inside lid-driven cavity was predicted using an alternative numerical scheme of the lattice Boltzmann. The advection term in the governing equation was solved using the constrained interpolated profile method. The capability of the scheme in solving the problem in hand has been proved. Detailed studies of cavity flow problem using the proposed approach have shown that the method is accurate and suitable for a wide range of Reynolds numbers simulation. This verification gave us confidence to apply the method to shallow lid-driven cavity flow problems. Complex structure of vortex was successfully regenerated. These demonstrate the proposed scheme is a very efficient numerical method to study fluid in an enclosed cavity and shall be applied to complex system in near future.

Acknowledgement

The authors would like to thank Universiti Teknologi Malaysia and Malaysia government for supporting these research activities.

References:

[1] F. Nathan and H. Richard, Simulating Acoustic Propagation using a Lattice Boltzmann Model of Incompressible Fluid Flow, *WSEAS Transactions on Signal Processing*, Vol.2, No.6, 2006, pp. 876-881.

[2] S. Chen and G. Doolen, Lattice Boltzmann Method for Fluid Flows, *Annual Review of Fluid Mechanics*, Vol.30, No.1, 1998, pp. 329-364.

[3] G. Breyiannis and D. Valougeorgis, Lattice Kinetic Simulations in Three-Dimensional Magnetohydrodynamics, *Physical Review E*, Vol.69, No.6, 2004, pp. 065702/1-065702/4.

[4] U. Frish, B. Hasslacher and Y. Pomeau, Lattice Gas Automata for the Navier-Stokes Equation, *Physical Review Letters*, Vol.56, No.14, 1986, pp. 1505-1508.

[5] X. He and L. S. Luo, A Priori Derivation of the Lattice Boltzmann Equation, *Physics Review E*, Vol.56, No.6, 1997, pp. 6811-6817.

[6] T. Abe, Derivation of the Lattice Boltzmann Method by Means of the Discrete Ordinate Method for the Boltzmann Equation, *Journal of Computational Physics*, Vol.131, No.1, 1997, pp.241-246.

[7] M. B. Reider and J. D. Sterling, Accuracy of Discrete-Velocity BGK Models for the Simulations of the Incompressible Navier-Stokes Equations, *Computers & Fluids*, Vol.24, No.4, 1995, pp. 456-467.

[8] N. Cao, S. Chen, S. Jin and D. Martinez, Physical Symmetry and Lattice Symmetry in the Lattice Boltzmann Method, *Physical Review E*, Vol.55, No.1, 1997, pp. R21-R24.

[9] R. Mei and W. Shyy, On the Finite Difference-Based Lattice Boltzmann Method in Curvilinear Coordinates, *Journal of Computational Physics*, Vol.134, No.2, 1997, pp. 306-315.

[10] J. Tolke, M. Krafczvk, M. Schulz, E. Rank and R. Berrios, Implicit Discritisation and Nonuniform Mesh Refinement approaches for FD Discretisations of LBGK Models, *International Journal of Modern Physics C*, Vol. 9. No.8, 1998, pp. 1143-1157.

[11] G. Hazi, A Nondispersive and Nondissipative Finite Difference Lattice Boltzmann Method, *International Journal of Modern Physics C*, Vol. 13. No.1, 2002, pp. 67-73.

[12] Y. B. Gan, A. G. Xu, G. C. Zhang, P. Zhang, L. Zhang and Y. J. Li, Finite-Difference Lattice Boltzmann Scheme for High Speed Compressible Flow: Two-Dimensional Case, *Communications in Theoretical Physics*, Vol. 50, No.1, 2008, pp. 201-210.

[13] T. Nakamura and T. Yabe, Cubic Interpolated Interpolation Scheme for Solving the Hyper Dimensional Vlasov-Poisson Equation in Phase Space, *Computer Physics Communications*, Vol.120, No.2, 1999, pp. 122-154.

[14] U. Ghia, K. N. Ghia amd C. Y. Shin, High-Re Solutions for Incompressible Flow using the Navier-Stokes Equations and Multigrid Method, *Journal of Computational Physics*, Vol.48, No.3, 1982, pp.387-411.

[15] C.S Nor Azwadi and S.M.R. Attarzadeh, An Accurate Numerical prediction of Solid Particle Fluid Flow in a Lid-driven Cavity, *International Journal of Mechanics*, Vol.5, No.3, 2011, pp. 123-128.

[16] C. S. Nor Azwadi and M.S. Idris, Mesoscale Numerical Approach to Predict Macroscale Fluid Flow Problems, *Journal of Applied Science*, Vol. 10, No. 15, 2010, pp. 1511-1524.

[17] P.L. Bhatnagar, E.P. Gross and M. Krook, A Model for Collision Process in Gasses. 1. Small Amplitude Processes in Charged and Neutral One-Component System, *Physical Review*, Vol.70, No.3, 1954, pp. 511-525.

[18] M.A. Mohd Irwan, A.M. Fudhail, C.S. Nor Azwadi and G. Masoud, Numerical Investigation of Incompressible Fluid Flow through Porous Media in a Lid-Driven Square Cavity, *American Journal of Applied Science*, Vol. 7, No. 10, 2010, pp. 1341-1344.

[19] C.S. Nor Azwadi and T. Tanahashi, Simplified Finite Difference Thermal Lattice Boltzmann Method, *International Journal of Modern Physics B*, Vol.22, No.22, 2008, pp. 3865-3876.

[20] T. Yabe, H. Mizoe, K. Takizawa, H. Moriki, H. N. Im and Y. Ogata, Higher-Order Schemes with CIP Method and Adaptive Soroban Grid towards Mesh Free Scheme, *Journal of Computational Physics*, Vol.194, No.1, 2004, pp. 57-77.

[21] C. S. Nor Azwadi, A. R. Mohd Rosdzimin, M. H. Al-Mola, Constrained Interpolated Profile for Solving BGK Boltzmann Equation, *European Journal of Scientific Research*, Vol.35, No.4, 2009, pp. 559-569.

[22] S. Hou, Q. Zou, S. Chen, G. Doolen and A. C. Cogley, Simulation of Cavity Flow by the Lattice Boltzmann Method, *Journal of*

Computational Physics, Vol.118, No.2, 1995, pp. 329-347.

[23] B. Abdelhadi, G. Hamza, B. Razik and E. Raouache, Natural Convection and Turbulent Instability in Cavity, *WSEAS Transactions on Heat and Mass Transfer*, Vol.1, No.2, 2006, pp. 179-184.